Rapid Communications

Proximity induced time-reversal topological superconductivity in Bi_2Se_3 films without phase tuning

Oscar E. Casas,[1,2] Liliana Arrachea,[3] William J. Herrera,[1] and Alfredo Levy Yeyati[2]

[1]*Departamento de Física, Universidad Nacional de Colombia, Bogotá, Colombia*

[2]*Departamento de Física Teórica de la Materia Condensada C-V, Condensed Matter Physics Center (IFIMAC) and Instituto Nicolás Cabrera, Universidad Autónoma de Madrid, E-28049 Madrid, Spain*

[3]*International Center for Advanced Studies, Escuela de Ciencia y Tecnología, Universidad Nacional de San Martín-UNSAM, Avenida 25 de Mayo y Francia, 1650 Buenos Aires, Argentina*

(Received 3 December 2018; published 23 April 2019)

Many proposals to generate a time-reversal invariant topological superconducting phase are based on imposing a π-phase difference between the superconducting leads proximitizing a nanostructure. We show that this phase can be induced on a thin film of a topological insulator such as Bi_2Se_3 in proximity to a *single* s-wave superconductor. In our analysis we take into account the parity degree of freedom of the electronic states which is not included in effective Dirac-like surface theories. We find that the topological phase can be reached when the induced interparity pairing dominates over the intraparity one. Application of an electric field perpendicular to the film extends the range of parameters where the topological phase occurs.

DOI: 10.1103/PhysRevB.99.161301

Introduction. The interest in topological phases of matter and, in particular, in topological superconductors (TSs) has not ceased to grow [1]. In addition to their fundamental interest, TSs are predicted to host topologically protected Majorana zero modes (MZMs) at the edges with potential applications in future quantum technologies [2].

Although topological superconductivity is expected to occur spontaneously in certain compounds such as Sr_2RuO_4 [3], actual vigorous experimental progress is coming from the side of artificial nanostructures. In particular, clear signatures of MZMs have been demonstrated in hybrid nanostructures combining semiconducting nanowires with a strong spin orbit (such as InAs or InSb) and conventional superconductors [4–8].

As in the case of other proposals based on arrays of magnetic impurities [9], these platforms constitute a realization of broken-time reversal (symmetry class D) one-dimensional (1D) topological superconductivity. Although the time-reversal counterpart or class DIII superconductivity has attracted great theoretical interest [10], its actual realization is still an experimental challenge. The zero-energy excitations in this class of TSs are Kramers pairs of Majorana modes. While their braiding properties appear to be path dependent [11,12], they exhibit other exotic transport [13,14] and spin [15–18] properties which render them objects of fundamental interest.

Intrinsic DIII superconductivity in two- and three-dimensional systems has been discussed in the literature (see, for instance, Refs. [19–21]), but also in this case most theoretical proposals have been focused on proximitized nanostructures. These, in general, require two basic ingredients: a multichannel or multiband electronic structure and a mechanism for inducing opposite pairing amplitudes on these channels [22]. These include Rashba nanowires proximitized by a d wave [23] or an iron-based superconductor with $s_\pm$ pairing symmetry [24], or two parallel nanowires with interwire pairing [25–27] or subject to opposite Zeeman fields [28]. Another scenario is spin orbit and many-body interactions in proximity with ordinary superconductivity [29,30]. Induction of the DIII phase on the edge or surface states of a 2D or a 3D topological insulator (TI) has also been considered [26,31–35]. References [33,35] suggest that for the case of a thin 3D

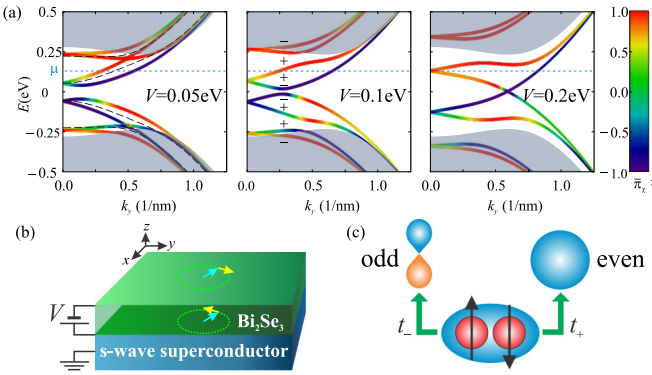

FIG. 1. (a) Surface state bands along k_y (with $k_x = 0$) in a thin Bi_2Se_3 film in the presence of an electric field, controlled by the biasing potential V between the top and bottom surfaces. The bands are helicity degenerate for $V = 0$ (dashed lines in left panel) but the degeneracy is broken for finite V. The signs in the middle panel indicate the band helicity and the color scale of the lines is set by the normalized relative weight $\bar{\pi}_\chi$ of the surface states on the two parity sectors [with $\bar{\pi}_\chi = 2\pi_\chi/(1+\pi_\chi^2)$, where π_χ is the relative weight defined in the main text]. The gray areas indicate the regions for the bulk states and the dashed horizontal line indicates the position of the chemical potential. (b) Geometry considered for analyzing the proximity effect. (c) Schematic representation of the interparity pairing which can be induced from the s-wave superconductor.

TI film, reaching the DIII phase requires forming a S/TI/S junction and imposing a π-phase difference. These studies are based on effective 2D models describing the surface states on the 3D TI film. In Ref. [35] the case of coupling to a single superconductor but including intersurface pairing is also considered.

In the present Rapid Communication we propose an approach for the case of proximitized 3D TI thin films. In contrast to previous works which start from the projected 2D theory, we use a 3D model which keeps track of the parity degree of freedom. We show that the DIII-TS phase may arise naturally by proximity to a *single* s-wave superconductor when considering the presence of interparity pairing. We further show that the inclusion of an external electric field, breaking inversion symmetry, helps to stabilize this topological phase.

The main ingredients of the proposed mechanism are illustrated in Fig. 1. The surface states of a 3D TI are characterized by a well defined helicity, i.e., they are eigenstates of the helicity operator $\hat{h} = (\boldsymbol{\sigma} \times \mathbf{k}_\parallel)_z/k_\parallel$, where $\mathbf{k}_\parallel$ is the wave vector parallel to the surface and σ_α are Pauli matrices in spin space [36]. In addition, these states are also characterized by a certain parity pseudospin, which depends on the surface orientation and on the material. For instance, in films of the Bi_2Se_3 family grown along the c axis, states on opposite surfaces have opposite helicities and opposite parity pseudospin [37]. In sufficiently thin films, the surface states corresponding to opposite sides are not fully decoupled but hybridize to some extent [38,39] and the helicity degeneracy can be broken by an electric field perpendicular to the film, as illustrated in Fig. 1(a). Therefore, when one of the surfaces is in contact with a superconductor as in Fig. 1(b), superconductivity is induced into the two surfaces in both parity channels, as well as interparity, as schematically depicted in Fig. 1(c). Interestingly, the interparity component induced on each helical channel typically have opposite signs. Our goal is to show that for the case of an s-wave superconductor, the TS phase can be reached provided that the interparity component is large enough and inversion symmetry is broken.

Model for a TI film and proximity effect. The low-energy and long-wavelength electronic properties of a TI of the Bi_2Se_3 family can be described by the $\mathbf{k}\cdot\mathbf{p}$ Hamiltonian introduced in Ref. [36] in a basis of four states which are combinations of p_z orbitals on the Bi and Se sites with even and odd parities. For analyzing the proximity effect it is convenient to perform a unitary transformation [37,40] with respect to the model in Ref. [36] [see discussion in the Supplemental Material (SM) [41]], which yields

$$H^{3D} = \mathcal{M}(\mathbf{k})(\tau_z \otimes \sigma_0) + A_1 k_z(\tau_y \otimes \sigma_0) - A_2[k_x(\tau_x \otimes \sigma_y) - k_y(\tau_x \otimes \sigma_x)], \quad (1)$$

where $\mathcal{M}(\mathbf{k}) = M_0 - B_1 k_z^2 - B_2(k_x^2 + k_y^2)$ [42], while τ_α are Pauli matrices operating in parity space. This Hamiltonian commutes with the helicity operator, leading to the properties of the surface states commented above.

In order to describe the proximitized thin film we now switch into a tight-binding (TB) description of the electronic structure. For this purpose we follow Ref. [43] and introduce a cubic lattice with parameter $a \sim 1$ nm oriented along the c axis and consider the $\mathbf{k}\cdot\mathbf{p}$ Hamiltonian as a long-wavelength expansion of this TB model. We shall consider the case of films of thickness $L_z = N_z a$ and impose periodic boundary conditions on the x, y directions. In the basis, $\psi_{k_\parallel,i} = (c_{k_\parallel,i+\uparrow}, c_{k_\parallel,i+\downarrow}, c_{k_\parallel,i-\uparrow}, c_{k_\parallel,i-\downarrow})^T$, where $c^\dagger_{k_\parallel,i\tau\sigma}$ creates an electron with parallel momentum $\mathbf{k}_\parallel$ on the i layer within the film, parity τ, and spin σ. The TB model adopts the form $\hat{H}^{TB} = \sum_{k_\parallel,ij} \psi^\dagger_{k_\parallel,i} \hat{\mathcal{H}}(\mathbf{k}_\parallel)_{ij} \psi_{k_\parallel,j}$, where

$$\hat{\mathcal{H}}(\mathbf{k}_\parallel)_{ij} = \epsilon(\mathbf{k}_\parallel)(\tau_z \otimes \sigma_0)\delta_{ij} + \frac{A_2}{a}[\sin k_y a(\tau_x \otimes \sigma_x) - \sin k_x a(\tau_x \otimes \sigma_y)]\delta_{ij} + \frac{B_1}{a^2}(\tau_z \otimes \sigma_0) \times (\delta_{ij-1} + \delta_{ij+1}) - \frac{iA_1}{2a}(\tau_y \otimes \sigma_0)(\delta_{ij-1} - \delta_{ij+1}), \quad (2)$$

with $\epsilon(\mathbf{k}_\parallel) = M_0 - 2[B_2(2 - \cos k_x a - \cos k_y a) + B_1]/a^2$. Within this model the eigenstates are again helicity degenerate (with the helicity operator properly extended to the discrete case) but this degeneracy is broken when an electric field along the z direction, $\hat{\mathcal{V}}_{ij} = 2V[i - (N_z + 1)/2]/(N_z - 1)\delta_{ij}$, is introduced.

To include the effect of induced pairing correlations on the film we consider the Bogoliubov–de Gennes (BdG) Hamiltonian, expressed in the basis $\Psi^\dagger_j(\mathbf{k}_\parallel) = (\psi_{k_\parallel,j}, -i\sigma_y\psi_{-k_\parallel,j})$. It reads

$$\hat{\mathcal{H}}^{BdG}(k_\parallel)_{ij} = [\hat{\mathcal{H}}(\mathbf{k}_\parallel)_{ij} + \hat{\mathcal{V}}_{ij} - \mu] \otimes \eta_z + \hat{\Delta}_{ij} \otimes \eta_x, \quad (3)$$

where μ is the chemical potential, and η_j are Pauli matrices in the particle-hole space. Although this model allows for more general configurations we shall focus in this work on the case depicted in Fig. 1(b), where pairing is induced on the $i = 1$ layer only, i.e., $\hat{\Delta}_{ij} = \hat{\Delta}_1\delta_{i1}\delta_{ij}$. $\hat{\Delta}_1$ has *intra-* ($\Delta_\pm$) and *inter-* (Λ) parity components,

$$\hat{\Delta}_1 = \frac{\Delta_+}{2}(\tau_0 + \tau_z) + \frac{\Delta_-}{2}(\tau_0 - \tau_z) + \Lambda\tau_x. \quad (4)$$

The pairing potentials depend on the coupling of the TI with the superconductor underneath. As discussed in the SM [41], they would typically have the form $\Delta_\pm = \pi\rho_F t_\pm^2$ and $\Lambda = \pi t_+ t_- \rho_F$, where ρ_F is the superconductor Fermi level density of states and $t_\pm$ are hopping parameters coupling the TI orbitals with parity $\pm$ and the superconductor. These parameters might have opposite signs. In particular, when an ordinary superconductor is contacted to the bottom of the film, with the chosen basis orbitals we have $t_+t_- < 0$, which implies that Λ has an overall sign with respect to $\Delta_\pm$. On the contrary, when the superconductor is contacted to the top surface, $t_+t_- > 0$, and thus $\Delta_\pm$ and Λ have the same sign.

It should be stressed that the above expressions are fully compatible with time-reversal symmetry. Regarding the size of Λ, while a noninteracting model suggests $\Lambda \sim \sqrt{\Delta_+\Delta_-}$ (see SM [41]), the presence of even a mild local Coulomb repulsion on the Bi and Se sites, reducing the intraparity pairing, would yield the condition $\Lambda > \sqrt{\Delta_+\Delta_-}$ which is necessary for stabilizing the DIII-TS phase as we show below.

Topological invariant. In the limit of weak coupling, the topological character of the proximitized TI film can be fully

determined by the normal electronic properties at the Fermi level [44]. The Z_2 topological invariant introduced in Ref. [44] is given by

$$N = \prod_n [\mathrm{sgn}\langle\psi_n(k_{F,n})|\mathcal{T}\hat{\Delta}^\dagger|\psi_n(k_{F,n})\rangle]^{m_n}, \quad (5)$$

where $\mathcal{T} = \tau_0 \otimes i\sigma_y K$, with K denoting complex conjugation, is the time-reversal operator, n runs over all bands crossing the Fermi energy, m_n is the number of time-reversal invariant (TRI) points enclosed by a band n, and $|\psi_n(k_{F,n})\rangle$ is the eigenstate on band n at the Fermi surface. In TIs of the Bi_2Se_3 family the only TRI point enclosed by the surface bands is the Γ point so that $m_n = 1$. On the other hand, due to the gap isotropy, Eq. (5) can be evaluated along any direction in the k_x-k_y plane.

As a paradigmatic example we shall examine the case $N_z = 2$. Details on the calculations are presented in the SM [41], where we also discuss the peculiar $N_z = 1$ case. The spectrum for $N_z = 2$ consists of four bands with positive energy which, expanded in $\mathbf{k} \equiv \mathbf{k}_\parallel$, are given by

$$E_{\alpha,\chi}(k) = \sqrt{E_1^2 + 2\alpha F_\chi + A_\chi^2 + V^2}. \quad (6)$$

$\alpha = \pm 1$ is a band index, $E_1^2 = \epsilon_k^2 + B^2 + C^2$, $F_\chi = \sqrt{(BC - A_\chi V)^2 + \epsilon_k^2(V^2 + B^2)}$, $\epsilon_k = M_0 - 2B_1/a^2 + B_2k^2$, with $k = |\mathbf{k}|$ and we have defined the parameters as $A_\chi = \chi A_2 k$, $B = B_1/a^2$, and $C = A_1/2a$. The bands and their evolution with voltage V are shown in Fig. 1(a). We focus on a chemical potential μ as indicated in Fig. 1(a), intersecting the bands with $\alpha = -1$. A nontrivial value of the Z_2 invariant in the present case (i.e., $N = -1$) implies simply different signs of the projected pairing in the two helicity channels,

$$\langle\psi_\chi|\mathcal{T}\hat{\Delta}^\dagger|\psi_\chi\rangle = 2|D_+|^2\left(\Delta_+ + \Delta_-\pi_\chi^2\right)(1 - \beta_\chi\Lambda). \quad (7)$$

In this expression we have introduced the quantities D_+, $\pi_\chi = D_-/D_+$, and $\beta_\chi = 2\pi_\chi/(\Delta_+ + \Delta_-\pi_\chi^2)$, which are defined from the components of the eigenstates of $\hat{H}^{\mathrm{TB}}$ on the bottom surface, i.e., we have $|\psi_\chi\rangle = (\hat{D}_\chi, \hat{U}_\chi)^T$, where $\hat{U}_\chi = (U_+, U_-)^T \otimes \hat{\phi}_\chi$ and $\hat{D}_\chi = (D_+, D_-)^T \otimes \hat{\phi}_\chi$, and $\hat{\phi}_\chi$ are the eigenstates of the helicity operator, so that π_χ measures the relative weight of the two parity sector components on the bottom surface. We then see that for having a nontrivial value of the Z_2 topological invariant, the necessary (however not sufficient) condition is π_χ (or equivalently β_χ) having different signs for the two helicities. An analytic expression for π_χ is given in the SM [41].

As can be observed in Fig. 1(a), the $\bar{\pi}_\chi$ parameter evolves differently along the lowest bands with opposite helicities, which are split due to the action of the electric field. While it remains negative for the $\chi = -1$ band for all values of the chemical potential within the TI gap, in the $\chi = +1$ band it evolves from negative to positive above a certain critical value of the momentum. As a consequence, for a chemical potential within this energy range and depending on the bias potential V, the effective pairing of Eq. (7) may have different signs on the two helicity bands leading to a nontrivial value of the Z_2 invariant, provided that, in addition, $\beta_+ > 1/\Lambda$ (see SM [41] for further details). In the following we study the occurrence

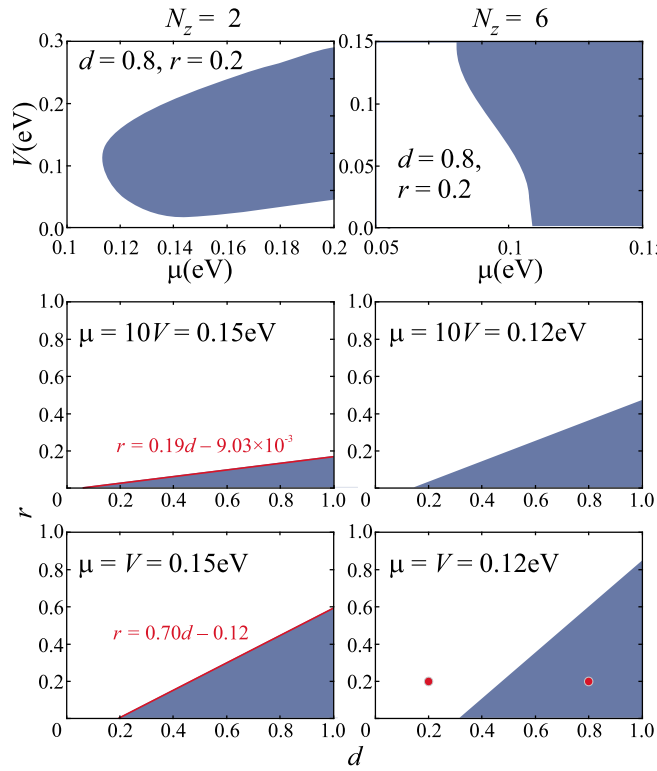

FIG. 2. Phase diagrams in the V, μ plane at fixed $r = 0.2$ and $d = 0.8$ (upper panels) and in the $r = \Delta_+/\Delta_-$, $d = \Lambda/\Delta_-$ plane at fixed $\mu = 10V$ (middle panels) and at $\mu = V$ (lower panels) for the cases $N_z = 2$ and $N_z = 6$. The dark (white) color indicates the topological (trivial) regions. As can be observed, larger values of V help to stabilize the topological phase for in a broader parameter region. The red lines in the d-r diagrams for the $N_z = 2$ case are the analytical prediction for the phase boundary as described in the SM [41].

of the TS phase as a function of the parameters $r = \Delta_+/\Delta_-$ and $d = \Lambda/\Delta_-$ which determine the relative size of the intra- and interparity pairing. We take $\Delta = \Delta_-$ as the reference energy.

In Fig. 2 we show the phase diagrams in the (μ, V) and in the (d, r) planes for the $N_z = 2$ and $N_z = 6$ cases. As can be observed in the upper panels, the topological phase appears for μ above a certain value which decreases for increasing N_z, corresponding to the closing of the hybridization gap between the surface states. On the other hand, μ should not exceed a value ~0.25 eV, where higher bands start to be populated. In addition, we observe that a finite V is needed in order to extend the stability of the topological phase in the (d, r) plane. For small V values (middle panels in Fig. 2) the stability is restricted to the regions $d \to 1$ and $r \to 0$, but these regions grow when $V \sim \mu$, gradually reaching the optimal case where the TS phase appears for $\Lambda > \sqrt{\Delta_+\Delta_-}$.

Another important aspect of the proximity effect in the TI film is the size of the induced gap parameter Δ_{ind}, which is determined by the smaller value of $|\langle\psi_\chi|\mathcal{T}\hat{\Delta}^\dagger|\psi_\chi\rangle|$ at the Fermi surface. As shown in Fig. 3(a), this quantity drops to zero at the boundary between the trivial and the TS region at the (d, r) plane, as expected for a topological transition, and

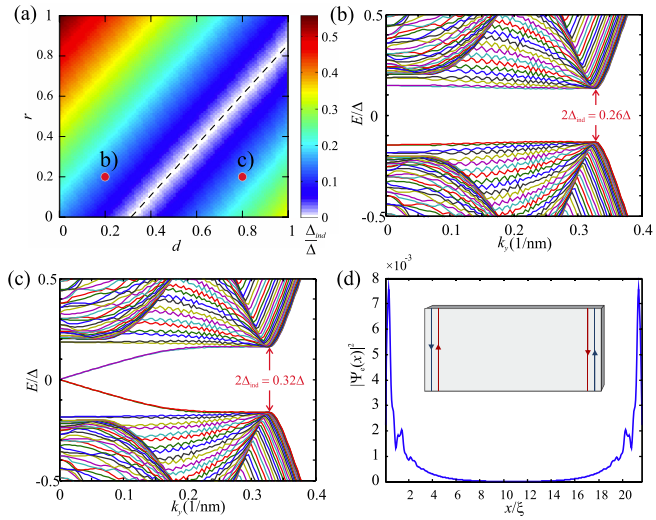

FIG. 3. (a) Induced gap Δ_{ind} in the (d, r) plane for the same parameters as in the lower right panel of Fig. 2. (b), (c) BdG spectrum for a slab of finite width $W \sim 20\xi$, where $\xi \sim A_2/\Delta$ is the coherence length in the TI film for the cases indicated by the red dots in (a). As can be observed, subgap states reaching zero energy for $k_y \to 0$ appear in the topological case. (b) Electron probability amplitude for these zero-energy states.

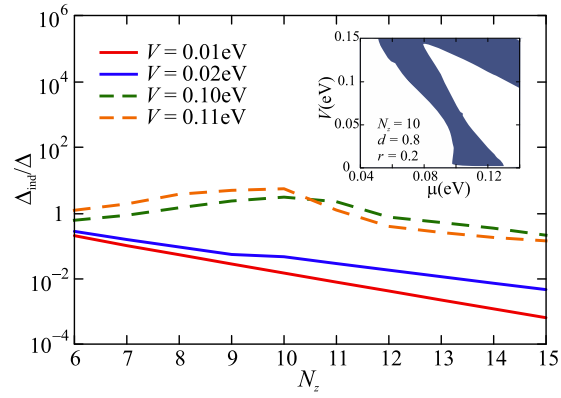

FIG. 4. Induced gap as a function of the TI layer thickness (N_z) for fixed $\mu = 0.04$ eV and different values of V. Solid and dashed lines indicate trivial and topological phases, respectively. The relative weight of the inter- and intraparity pairing at the bottom layer was fixed to $d = 0.8$ and $r = 0.2$. The inset shows the phase diagram in the μ-V plane for $N_z = 10$.

increases when departing from this boundary. The size of Δ_{ind} can be more clearly appreciated in Figs. 3(b) and 3(c) where we show the BdG spectrum for an $N_z = 6$ film of finite width in the x direction. The two cases correspond to parameters within the trivial and the topological regions, as indicated by the two dots in the lower right panel of Fig. 2 and in Fig. 3(a). In the former case the spectrum exhibits a pair of subgap states, dropping to zero energy for $k_y \to 0$. The corresponding wave function, exhibiting localization at the edges of the film, is plotted in Fig. 3(d). Notice that the localization length is of the order of 5ξ, which coincides with an effective coherence length $\xi_{\text{eff}} \sim A_2/\Delta_{\text{ind}}$. As expected for a TS-DIII phase, these states correspond to Kramers pairs of Majorana modes.

The above results correspond to very thin TI layers with $N_z \leqslant 6$. When N_z is further increased, the DIII-TS phase can still be reached for certain parameter values, but the topological region shrinks and the phase diagram starts to exhibit disconnected regions, as shown in the inset of Fig. 4 for $N_z = 10$. The behavior of the induced gap with N_z depends on the V value. While for small V values, i.e., outside the topological region, it decreases exponentially with N_z, for larger V it exhibits a nonmonotonic behavior, first increasing and eventually decreasing for $N_z \geqslant 10$, as can be observed in the main frame of Fig. 4. This behavior is associated with the fact that higher bands start to cross the chemical potential.

A word of caution is in order regarding the reliability of the precise quantitative predictions of our model, which can nevertheless be trusted at a qualitative level. It is also important to remark that when the film is contacted to a superconductor through both surfaces, thus recovering the inversion symmetry, the topological phase disappears [41].

Conclusions. We have shown that a time-reversal invariant TS phase can be induced on a TI film of the Bi_2Se_3 family proximitized by a conventional superconductor. In contrast to previous proposals, our mechanism does not rely on tuning the phase difference in a S/TI/S junction but arises from the induced interparity pairing which naturally occurs at the S/TI interface. The mechanism requires breaking the spatial inversion symmetry and a certain degree of hybridization between the TI surface states. Application of an electric field perpendicular to the layers helps to stabilize the TS phase for thicker films in a broader parameter space. Notice that such fields appear spontaneously at the interface between a TI film and its substrate due to charge accumulation [38].

As a final remark let us mention that proximitized Bi_2Se_3 films have been analyzed in several experiments, either through the Josephson effect [45,46] or by tunnel spectroscopy [47,48]. We hope that our work could motivate further experimental studies on these types of devices.

Acknowledgments. We thank L. Brey and J. Schmalian for useful comments on the manuscript. This work has been supported by Spanish MINECO through Grants No. FIS2014-55486-P and No. FIS2017-84860-R, and through the "María de Maeztu" Programme for Units of Excellence in R&D (MDM-2014-0377). L.A. is thankful for support from CONICET and SECyT from Argentina, as well as the Alexander von Humboldt Foundation from Germany. W.J.H. and O.E.C. acknowledge funding from COLCIENCIAS, Grant No. 110165843163 and Doctorate Scholarship No. 617.

[1] M. Sato and Y. Ando, Topological superconductors: A review, Rep. Prog. Phys. **80**, 076501 (2017).

[2] S. Vijay, T. H. Hsieh, and L. Fu, Majorana Fermion Surface Code for Universal Quantum Computation, Phys. Rev. X **5**,

041038 (2015); S. Plugge, A. Rasmussen, R. Egger, and K. Flensberg, Majorana box qubits, New J. Phys. **19**, 012001 (2017).

[3] A. P. Mackenzie and Y. Maeno, The superconductivity of Sr_2RuO_4 and the physics of spin-triplet pairing, Rev. Mod. Phys. **75**, 657 (2003).

[4] V. Mourik, K. Zuo, S. M. Frolov, S. R. Plissard, E. P. A. M. Bakkers, and L. P. Kouwenhoven, Signatures of Majorana fermions in in hybrid superconductor-semiconductor nanowire devices, Science **336**, 1003 (2012).

[5] A. Das, Y. Ronen, Y. Most, Y. Oreg, M. Heiblum, and H. Shtrikman, Zero-bias peaks and splitting in an Al-InAs nanowire topological superconductor as a signature of Majorana fermions, Nat. Phys. **8**, 887 (2012).

[6] S. M. Albrecht, A. P. Higginbotham, M. Madsen, F. Kuemmeth, T. S. Jespersen, J. Nyg, P. Krogstrup, and C. M. Marcus, Exponential protection of zero modes in Majorana islands, Nature (London) **531**, 206 (2016).

[7] M. Deng, S. Vaitiekenas, E. Hansen, J. Danon, M. Leijnse, K. Flensberg, J. Nygard, P. Krogstrup, and C. Marcus, Majorana bound state in a coupled quantum-dot hybrid-nanowire system, Science **354**, 1557 (2016).

[8] H. J. Suominen, M. Kjaergaard, A. R. Hamilton, J. Shabani, C. J. Palmstrøm, C. M. Marcus, and F. Nichele, Zero-Energy Modes from Coalescing Andreev States in a Two-Dimensional Semiconductor-Superconductor Hybrid Platform, Phys. Rev. Lett. **119**, 176805 (2017).

[9] S. Nadj-Perge, I. K. Drozdov, J. Li, H. Chen, S. Jeon, J. Seo, A. H. MacDonald, B. A. Bernevig, and A. Yazdani, Observation of Majorana fermions in ferromagnetic atomic chains on a superconductor, Science **346**, 602 (2014).

[10] For a recent review, see A. Haim and Y. Oreg, Time reversal-invariant topological superconductivity, arXiv:1809.06863.

[11] K. Wölms, A. Stern, and K. Flensberg, Local Adiabatic Mixing of Kramers Pairs of Majorana Bound States, Phys. Rev. Lett. **113**, 246401 (2014).

[12] K. Wölms, A. Stern, and K. Flensberg, Braiding properties of Majorana Kramers pairs, Phys. Rev. B **93**, 045417 (2016).

[13] J. Li, W. Pan, B. A. Bernevig, and R. M. Lutchyn, Detection of Majorana Kramers Pairs Using a Quantum Point Contact, Phys. Rev. Lett. **117**, 046804 (2016).

[14] C. Schrade and L. Fu, Parity-Controlled 2π Josephson Effect Mediated by Majorana Kramers Pairs, Phys. Rev. Lett. **120**, 267002 (2018).

[15] A. Keselman, L. Fu, A. Stern, and E. Berg, Inducing Time-Reversal-Invariant Topological Superconductivity and Fermion Parity Pumping in Quantum Wires, Phys. Rev. Lett. **111**, 116402 (2013).

[16] A. Camjayi, L. Arrachea, A. Aligia, and F. von Oppen, Fractional Spin and Josephson Effect in Time-Reversal-Invariant Topological Superconductors, Phys. Rev. Lett. **119**, 046801 (2017).

[17] M. Mashkoori, A. G. Moghaddam, M. H. Hajibabaee, A. M. Black-Schaffer, and F. Parhizgar, Impact of topology on the impurity effects in extended s-wave superconductors with spin-orbit coupling, Phys. Rev. B **99**, 014508 (2019).

[18] A. Aligia and L. Arrachea, Entangled end states with fractionalized spin projection in a time-reversal-invariant topological superconducting wire, Phys. Rev. B **98**, 174507 (2018).

[19] X.-L. Qi, T. L. Hughes, S. Raghu, and S.-C. Zhang, Time-Reversal-Invariant Topological Superconductors and Superfluids in Two and Three Dimensions, Phys. Rev. Lett. **102**, 187001 (2009).

[20] L. Fu and E. Berg, Odd-Parity Topological Superconductors: Theory and Application to $Cu_xBi_2Se_3$, Phys. Rev. Lett. **105**, 097001 (2010).

[21] M. S. Scheurer and J. Schmalian, Topological superconductivity and unconventional pairing in oxide interfaces, Nat. Commun. **6**, 6005 (2015).

[22] A. Haim, E. Berg, K. Flensberg, and Y. Oreg, No-go theorem for a time-reversal invariant topological phase in noninteracting systems coupled to conventional superconductors, Phys. Rev. B **94**, 161110(R) (2016).

[23] C. L. M. Wong and K. T. Law, Majorana Kramers doublets in $d_{x^2-y^2}$-wave superconductors with Rashba spin-orbit coupling, Phys. Rev. B **86**, 184516 (2012).

[24] F. Zhang, C. L. Kane, and E. J. Mele, Time-Reversal-Invariant Topological Superconductivity and Majorana Kramers Pairs, Phys. Rev. Lett. **111**, 056402 (2013).

[25] E. Gaidamauskas, J. Paaske, and K. Flensberg, Majorana Bound States in Two-Channel Time-Reversal-Symmetric Nanowire System, Phys. Rev. Lett. **112**, 126402 (2014).

[26] J. Klinovaja, A. Yacoby, and D. Loss, Kramers pairs of Majorana fermions and parafermions in fractional topological insulators, Phys. Rev. B **90**, 155447 (2014).

[27] H. Ebisu, B. Lu, J. Klinovaja, and Y. Tanaka, Theory of time-reversal topological superconductivity in double Rashba wires: symmetries of Cooper pairs and Andreev bound states, Prog. Theor. Exp. Phys. **2016**, 083I01 (2016).

[28] C. Reeg, C. Schrade, J. Klinovaja, and D. Loss, DIII topological superconductivity with emergent time-reversal symmetry, Phys. Rev. B **96**, 161407(R) (2017).

[29] A. Haim, A. Keselman, E. Berg, and Y. Oreg, Time-reversal invariant topological superconductivity induced by repulsive interactions in quantum wires, Phys. Rev. B **89**, 220504(R) (2014).

[30] A. Haim, K. Wölms, E. Berg, Y. Oreg, and K. Flensberg, Interaction-driven topological superconductivity in one dimension, Phys. Rev. B **94**, 115124 (2016).

[31] L. Fu and C. Kane, Superconducting Proximity Effect and Majorana Fermions at the Surface of a Topological Insulator, Phys. Rev. Lett. **100**, 096407 (2008).

[32] L. Santos, T. Neupert, C. Chamon, and C. Mudry, Superconductivity on the surface of topological insulators and in two-dimensional noncentrosymmetric materials, Phys. Rev. B **81**, 184502 (2010).

[33] C. X. Liu and B. Trauzettel, Helical Dirac-Majorana interferometer in a superconductor/topological insulator sandwich structure, Phys. Rev. B **83**, 220510(R) (2011).

[34] C. Schrade, A. A. Zyuzin, J. Klinovaja, and D. Loss, Proximity-Induced π Josephson Junctions in Topological Insulators and Kramers Pairs of Majorana Fermions, Phys. Rev. Lett. **115**, 237001 (2015).

[35] F. Parhizgar and A. M. Black-Schaffer, Highly tunable time-reversal-invariant topological superconductivity in topological insulator thin films, Sci. Rep. **7**, 9817 (2017).

[36] H. Zhang, C.-X. Liu, X.-L. Qi, X. Dai, Z. Fang, and S.-C. Zhang, Topological insulators in Bi_2Se_3, Bi_2Te_3, and Sb_2Te_3

with a single Dirac cone on the surface, Nat. Phys. **5**, 438 (2009).

[37] C.-X. Liu, X.-L. Qi, H. Zhang, X. Dai, Z. Fang, and S.-C. Zhang, Model Hamiltonian for topological insulators, Phys. Rev. B **82**, 045122 (2010).

[38] Y. Zhang *et al.*, Crossover of the three-dimensional topological insulator Bi_2Se_3 to the two-dimensional limit, Nat. Phys. **6**, 584 (2010).

[39] H.-Z. Lu, W.-Y. Shan, W. Yao, Q. Niu, and S.-Q. Shen, Massive Dirac fermions and spin physics in an ultrathin film of topological insulator, Phys. Rev. B **81**, 115407 (2010).

[40] P. G. Silvestrov, P. W. Brouwer, and E. G. Mishchenko, Spin and charge structure of the surface states in topological insulators, Phys. Rev. B **86**, 075302 (2012).

[41] See Supplemental Material at http://link.aps.org/supplemental/10.1103/PhysRevB.99.161301 for details of the model Hamiltonian, the origin of the inter parity pairing and details of the Z_2 invariant in the $N_z = 1, 2$ cases.

[42] According to Ref. [37], appropriate parameters for Bi_2Se_3, obtained from fits to *ab initio* calculations, are $M_0 = 0.28$ eV, $A_1 = 2.26$ eV Å, $A_2 = 3.33$ eV Å, $B_1 = 6.86$ eV Å^2, and $B_2 = 44.5$ eV Å^2.

[43] S. Acero, L. Brey, W. J. Herrera, and A. Levy Yeyati, Transport in selectively magnetically doped topological insulator wires, Phys. Rev. B **92**, 235445 (2015).

[44] X.-L. Qi, T. L. Hughes, and S.-C. Zhang, Topological invariants for the fermi surface of a time-reversal-invariant superconductor, Phys. Rev. B **81**, 134508 (2010).

[45] J. R. Williams, A. J. Bestwick, P. Gallagher, S. S. Hong, Y. Cui, A. S. Bleich, J. G. Analytis, I. R. Fisher, and D. Goldhaber-Gordon, Unconventional Josephson Effect in Hybrid Superconductor-Topological Insulator Devices, Phys. Rev. Lett. **109**, 056803 (2012).

[46] M. Snelder, C. G. Molenaar, Y. Pan, D. Wu, Y. K. Huang, A. de Visser, A. A. Golubov, W. G. van der Wiel, H. Hilgenkamp, M. S. Golden, and A. Brinkman, Josephson supercurrent in a topological insulator without a bulk shunt, Supercond. Sci. Technol. **27**, 104001 (2014).

[47] F. Yang *et al.*, Proximity-effect-induced superconducting phase in the topological insulator Bi_2Se_3, Phys. Rev. B **86**, 134504 (2012).

[48] A. Finck, C. Kurter, Y. Hor, and D. Van Harlingen, Phase Coherence and Andreev Reflection in Topological Insulator Devices, Phys. Rev. X **4**, 041022 (2014).